Version of Record: https://www.sciencedirect.com/science/article/pii/S0149197022000890
Manuscript_80c40fa478c81a9913141dfa700acc5b

Experimental Investigations of Critical Heat Flux Re-Occurrence on Post-CHF Surfaces

Mingfu He[1], Amir Ali[2], and Minghui Chen[1*]

[1]: Department of Nuclear Engineering, University of New Mexico, Albuquerque, NM, USA 87131
[2]: Department of Nuclear Engineering, Idaho State University, Idaho Falls, ID, USA 83401

ABSTRACT

Under the extreme environments of light water reactors, the cladding materials demonstrate evolutionary transformations in terms of material compositions, surface morphologies, and thermal-physical properties. This study investigates how the temperature overshooting of Critical Heat Flux (CHF) affects the re-occurrence of CHF on the post-CHF surfaces. Experimental results reveal that the CHF difference between as-received and post-CHF surfaces can be significant, which depends on materials. CHF is enhanced on post-CHF Stainless Steel (SS 316) specimens while it deteriorates on post-CHF Inconel-600 specimens. In comparison with the as-received surfaces, the post-CHF surface of SS 316 is more hydrophobic, while Inconel 600 is more hydrophilic. The scanning electron microscope micrographs of post-CHF surfaces show that surface morphologies that are structured by oxide crystals are formed on SS 316 samples but not on Inconel 600 samples. The physical rationale behind the CHF difference could be boiling heat transfer conjugated with thermal-physical proprieties of investigated surface materials and surface morphologies features. The results imply that it is indispensable to bookkeep the evolutionary changes of cladding surface materials, especially for cladding candidates of Accident Tolerant Fuel since operation histories can leave footprints on cladding surfaces, thus resulting in differences in CHF re-occurrences.

KEYWORDS

Critical Heat Flux, Surface Wettability, Post-CHF Surfaces, and Evolutionary Changes.

ACRONYMS

ATF: Accident Tolerant Fuel
CHF: Critical Heat Flux (kW/m^2)
DC: Direct Current
DNB: Departure from Nucleate Boiling
LOCA: Loss of Coolant Accident
LWR: Light Water Reactor
ONB: Onset of Nucleate Boiling
PCT: Peak Cladding Temperature
SEM: Scanning Electron Microscope
SS: Stainless Steel

1 INTRODUCTION

Critical Heat Flux (CHF) and Departure from Nucleate Boiling (DNB) demarcate the power limit of nuclear reactor cores and heat exchangers (Chen et al., 2018), marked by a sudden temperature overshooting on cladding surface. At the snapshot moment of CHF occurrence, the rapid spatial and temporal variation of surface temperature is the primary physical rationale behind the instantaneous transition from nucleate boiling to film boiling (Carrica et al., 1995). It was believed that the CHF occurrence and the boiling regime transition were contributed by far-field properties such as pressure, mass flux, and the equilibrium quality (He and Lee, 2018). More recent CHF experiments have shown that the near-field properties, including material compositions and morphologies of heat transfer surface (Morshed et al., 2013), also have influential impacts on CHF. However, the physical rationales behind the effects of material-related factors on CHF remain still controversial and ambiguous. In recent years, experimental investigations on the effects of surface oxidization on boiling heat transfer have gained more and more research attention in thermal management systems because of their implications to safety risk assessments, especially in nuclear reactor cores.

During the fuel cycle of light water reactors (LWRs), cladding materials are exposed to high temperature water/steam mixture and radiation doses. This definitely results in surface characteristics changes of cladding materials such as formation of oxide layers (Cheng et al., 2012) and surface wettability enhancement (Ali et al., 2018). Some preliminary experimental studies have already revealed that the presence of an oxide layer has significant impacts on CHF. For instance, the oxidized zircaloy-4 has about 40% enhancement of pool boiling CHF compared to the non-oxidized surface (Lee et al., 2015), while the oxide layer of SA508 steel alloy showed an adverse effect on pool boiling CHF (Son et al., 2016). Their theoretical rationales behind CHF enhancement and deterioration are completely different. Lee et al. (2015) considered the better surface wettability of oxidized sample as the primary contributor to CHF enhancement. On the contrary, Son et al. (2016) thought that the presence of magnetite layer might deteriorate lateral heat dissipation near CHF and result in adverse impacts on CHF. Besides pool boiling study, Trojer et al. (2018) experimentally proved that the oxide layer of low-carbon steel would make boiling surfaces super-hydrophilic and thus be more capable of wicking water, further rendering 70% enhancement of flow boiling CHF in comparison to SS-316. Wang et al. (2020) also showed that the increase of boiling cycle would result in higher flow boiling CHF of carbon steel for the oxidation effect on the cooling ability of reactor pressure vessel downward-faced wall. Those studies imply that the evolutions of reactor core materials may contribute to variations of safety margin at the different stages during the LWR fuel cycle. Although the thickness of oxide layer varies from several microns to several dozens of microns, their significant impacts on boiling heat transfer are evidently obvious. This cannot be sufficiently resolved by the present mechanistic views, including the hydrodynamics and nucleate site theories. Thus, the experimental investigations on such effects seem the only feasible solution to analyzing the potential thermal risks resulting from surface oxidization. Yeom et al. (2020) measured the static contact angles of four different tested materials with three surface finish conditions, and their results showed that the tested samples of SiC and Zircaloy-4 had greater contact angles after pool boiling CHF oxidization while the contact angles of oxidized FeCrAl and Cr-coated samples decreased in comparison with their as-prepared counterparts. Umretiya et al. (2020) also demonstrated that Cr-coated Zircaloy-4 samples that had been exposed in water/air showed the increasing behavior of

contact angle as the increasing of the exposure time. Those experimental results imply that the oxidized samples can not 100% guarantee the decreasing of the contact angle or enhance the surface wettability. Not only are there controversial points on the surface wettability change on oxidized surfaces, but also the physical mechanisms behind the enhancement/deterioration of oxide layer on pool boiling CHF still remain ambiguous and critically debated in the boiling heat transfer community. Because experimental results and the proposed rationales reported in various studies conflict with each other. For example, Lee and Chang (2012) and Mei et al. (2018) reported that the presence of oxide layers contributed to the pool boiling CHF of SA 508, and the enhancement effect was progressively augmented as the increase of the oxidization time. However, Son et al. (2016) found that the pool boiling CHF of SA 508 was deteriorated due to the surface oxidization of SA 508, and the deterioration effect was not enhanced over the increasing of oxidization time. In light of the results, the mechanistic rationales behind the enhancement of oxide layer on flow boiling CHF of SS 316 are not evidently clear because it is difficult to separate multiple physical mechanisms that act on the trigger of CHF occurrence, such as the variations of material thermal-physical properties, surface roughness, capillary wickability, surface wettability, and porous microstructures.

How evolutionary histories of cladding materials affect the thermal-hydraulic performance of themselves is important to the precaution of accident scenarios, especially the impacts of oxide layers on CHF. The core loading of Accident Tolerant Fuel (ATF) is also in need of knowledge about how the evolutionary changes of ATF cladding affect thermal-hydraulic performances of LWRs. Since the advent of ATF cladding, the one of its primary functionalities is to minimize the failure probability of cladding integrity, such as burst and crack (Zinkle et al., 2014). Although cladding materials can survive from accidental scenarios such as loss-of-coolant accident (LOCA) and remain intact in structural integrity, it is still indispensable to recheck the safety margin of oxidized ATF claddings. Motivated by the need to fill this gap, this study experimentally explores how the effects of oxide layers on CHF respond to variations of inlet subcooling and mass flux using SS 316 tubes. This can give us a potential guideline to large lab-scale boiling experiments of ATF oxidized claddings. The rest of this paper is organized as follows, Section 2 briefly describes the experimental methods and facilities, Section 3 presents experimental results and their implications discussions, and some concluding remarks are made in Section 4.

2 EXPERIMENTAL METHODOLOGIES

2.1 Flow Boiling Facilities and Procedures

CHF experiments of flow boiling are performed for the steady-state condition in the flow loop, as shown in Fig. 1. This flow boiling facility is composed of a pressurized water tank isolating steam from the water flow, a circulation pump driving flow and controlling mass flow rate, a preheater adjusting the inlet temperature of the working fluid, a chiller cooling down the system temperature, a test section for testing different cladding materials, various instrumentation measuring pressures, temperatures, and mass fluxes, transducers for obtaining currents and voltage drops at the test section. The flow loop is made of SS 316, and the working fluid is the deionized water.

The experimental system is designed as the internal upward flow configuration. The circular tube with a length of 21.5 inches, an outer diameter of 0.375 inches and a wall thickness of 0.02 inches is vertically connected to two orifice fittings. A schematic of the test section is shown in Fig. 2.

The entrance length is greater than 15 inches to ensure the fully developed water flow based on Olson and Sparrow's correlation (Olson and Sparrow, 1963). The test section is uniformly heated by the direct joule heating powered by a direct current power supply. The actual heated length is two inches and is wrapped by a pad of thermal insulation foam to reduce the heat loss to the surroundings. It is noted that this pad of thermal insulation foam is made from three different material wrappers, respectively stacked from the innermost to the outmost layers, a high-temperature tolerant duct tape, a thick layer of mineral wool and a thin layer of flexible foam cloth. The purpose of three different materials being stacked in layers is that the innermost duct tape is used to fix thermocouples tightly on the cladding surface, a thick layer of mineral wool serves thermal insulation and minimizes heat loss to the ambient environment, and the outmost flexible foam cloth is used to tightly mount the mineral wool on the cladding surface. Two T-type thermocouples and two pressure transducers are installed upon two orifice tube fittings to measure temperatures and pressures at both inlet and outlet, respectively. Eight K-type thermocouples are placed at the outer tube surface in pairs to measure the outer surface temperatures axially. To minimize the contact resistance of the electric current at the junction from power terminals to the tested tube, a very high electrically conductive epoxy is spread all over the contacting surfaces.

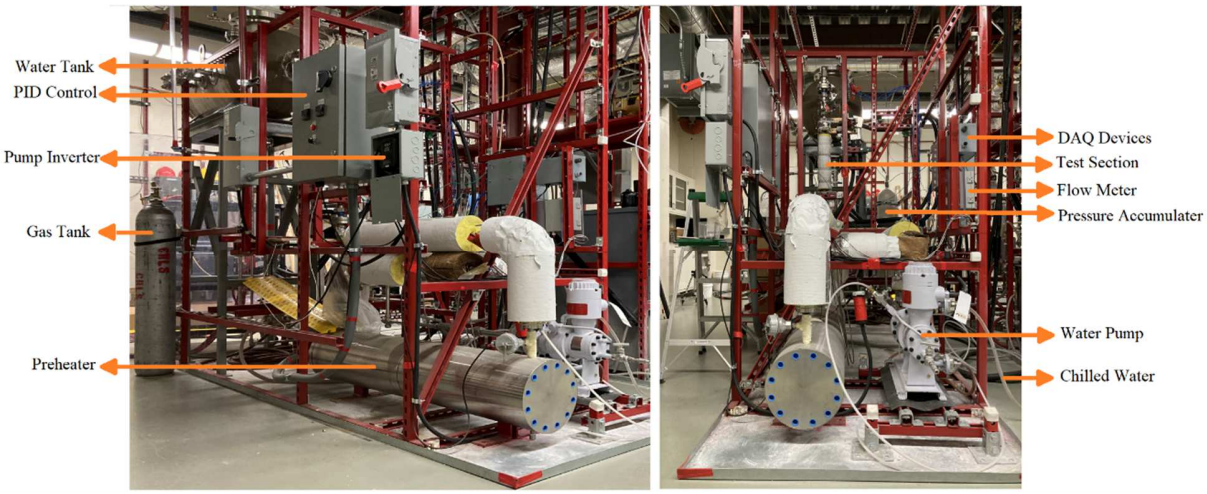

Fig. 1. Photos of the Flow Boiling Test Facility.

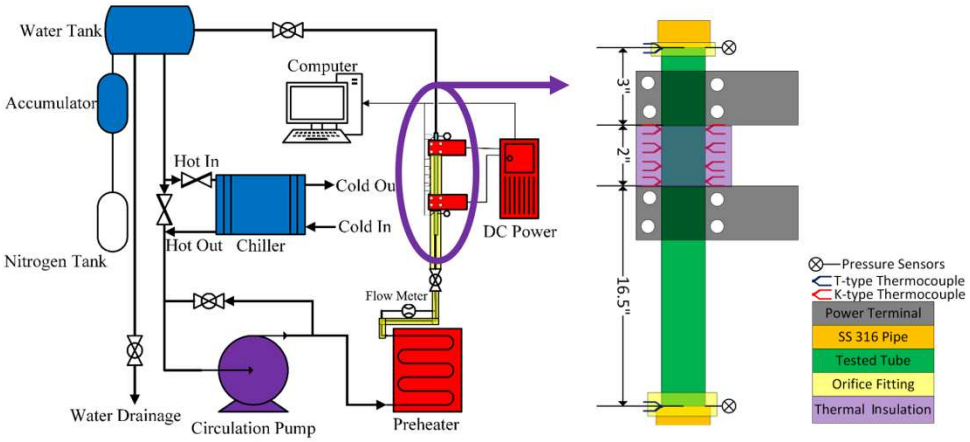

Fig. 2. Schematic of the Flow Boiling Loop and the Test Section.

Before directly applying power to the test section, the working fluid is heated up to 94 °C for at least 30 minutes with the intention of degassing dissolved air, then the temperature of working fluid is reduced by the chiller and preheater to the specified inlet temperature. For the signifier of the steady-state condition, this experimental study adopts the following criterion such that the temperature difference between two consecutive mean temperatures measured at a point is less than 0.5 °C, the mean temperature at a point is averaged by a time series of 30 measured temperatures points and all eight measured points are supposed to have the temperature difference less than 0.5 °C. If this criterion is satisfied, then the present test section will be treated under the steady-state condition, and then the heat flux will be incremented by increasing the DC power current by a step size of 1 A, corresponding to an approximate 4-W power step increase. As for the detection mechanism of CHF in this study, a moment when the temperature difference is greater than 30 °C is marked as CHF occurrence. Then the system will immediately shut down the power supply.

2.2 Test Materials and Experimental Setup

The test tubes are rinsed sequentially with acetone, methanol, and distilled water to remove any contamination on the internal surface. The internal surfaces of the tested specimen are polished by 320 grit sandpapers for the consistency of surface morphologies. Then the tested specimen is washed by distilled water flow that is agitated by ultrasound to detach the abrasive particles of sandpaper from the internal surfaces of tested materials. The selected materials of tested tubes are SS 316 and Inconel 600 because these materials have a relatively high electrical resistance and can reach the power level required for CHF being occurred.

All the flow boiling experiments are conducted under the atmospheric pressure of Albuquerque of 84 kPa. The inlet subcooling (ΔT_{sub}) ranges from 0 to 30 °C by a step of 5 °C. The mass flux varies from 300 to 3000 kg/m^{2}s.

2.3 CHF Measurement Uncertainties

There are three different wrappers of thermal insulation in the test section to ensure negligible heat loss. The heat flux of the tested section can be calculated as follows,

$$q'' = \frac{VI}{\pi(OD-2WT)L} \tag{1}$$

where V is the voltage drop across the test section, I is the power current passing through the test section, and L is the actual heated length of the tested section, OD and WT denote the outer diameter and wall thickness of the tube, respectively. The corresponding uncertainty of heat flux is expressed as,

$$\frac{|\Delta q''|}{q''} = \sqrt{(\frac{\Delta V}{V})^2 + (\frac{\Delta I}{I})^2 + (\frac{\Delta OD}{OD})^2 + 4(\frac{\Delta WT}{WT})^2 + (\frac{\Delta L}{L})^2}\ . \tag{2}$$

The measurement uncertainties of voltage drop, power current, and the actual heated length are 0.0054, 0.0051, and 0.0034, respectively. Based on those uncertainties, the measurement uncertainty of heat flux is 0.1064. The measurement uncertainty of self-adhesive K-type thermocouples is ±1.1 °C according to the vendor, Omega Engineering Inc.

3 RESULTS ANALYSES AND DISCUSSIONS

Experimental results show how a sudden temperature overshoot led by CHF occurrence affects flow boiling behavior in tubes.

3.1 Impacts of Temperature Overshoot Footprints on CHF

In this study, the temperature difference between the surface temperature at the outlet location and the liquid temperature at the inlet is adopted to present the boiling curves under different flow boiling conditions. The fresh tubes are the as-received tubes that are only blasted by the sandpaper for the surface consistency without undergoing the flow boiling heat transfer tests, and the oxidized tubes are those tested tubes where CHF occurred on at least once.

It can be noted from Fig. 3 that the flow boiling CHF of oxidized SS 316 tube is significantly improved in comparison with that of fresh SS 316 tube under the mass flux of 300 kg/m^{2}s and inlet subcooling of 0 °C. In addition, the ONB of the oxidized SS 316 tube could be enhanced in comparison that of the fresh SS 316 tube. These two important points marked by the nucleate boiling stage are greatly promoted, further implying that the thermal economy of nucleate boiling heat transfer can be reinforced. The experimental observations of intensifications of ONB and CHF can be universally found in other flow boiling cases, as shown in Figs. 4, 5, and 6.

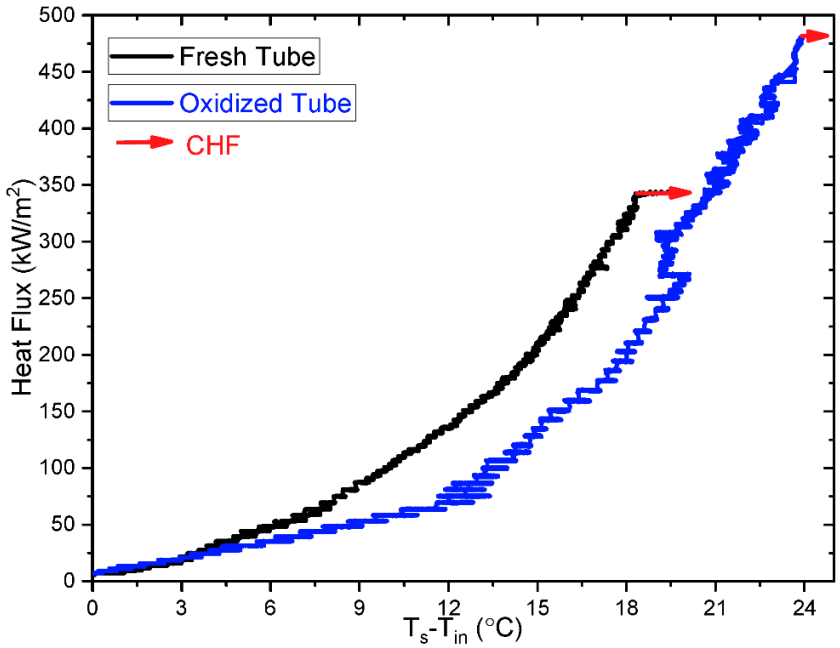

Fig. 3. Flow Boiling Curve of Fresh and Oxidized SS 316 Tubes with G = 300 kg/m^{2}s and ΔT_{sub}= 0 °C.

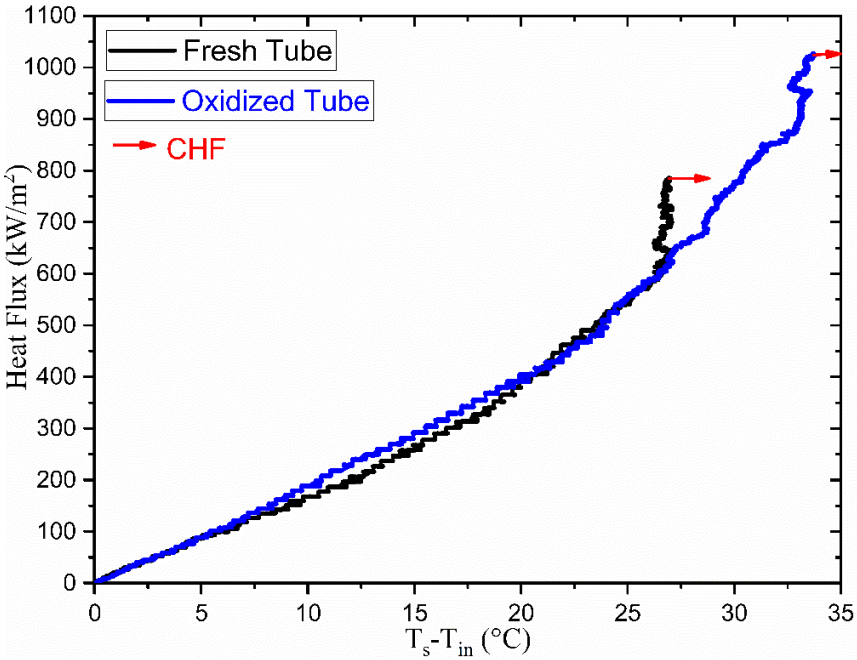

Fig. 4. Flow Boiling Curve of Fresh and Oxidized SS 316 Tubes with G = 2000 kg/m^{2}s and ΔT_{sub} = 0 °C.

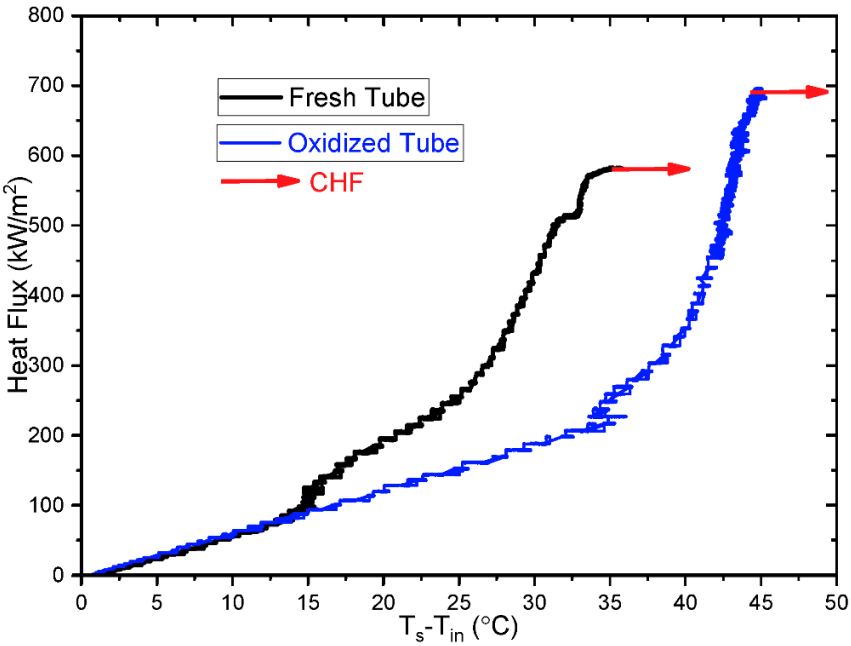

Fig. 5. Flow Boiling Curve of Fresh and Oxidized SS 316 Tubes with G = 500 kg/m^{2}s and ΔT_{sub} = 10 °C.

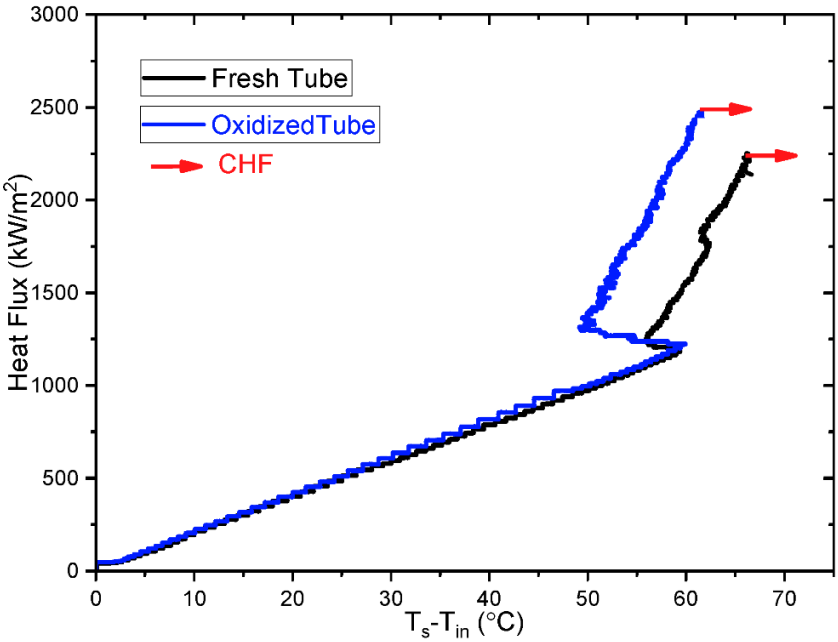

Fig. 6. Flow Boiling Curve of Fresh and Oxidized SS 316 Tubes with G = 2500 kg/m^{2}s and ΔT_{sub} = 10 °C.

The contributions by mass flux and inlet subcooling to ONB and CHF can be explained by the far-field mechanistic views of mass, momentum, and energy. However, the physical rationales behind the CHF enhancements on the used tubes that were oxidized by CHF occurrence could be attributed to the formation of an oxide layer on the tube surfaces. This could be seen from previous CHF experiments of pool boiling (Kam et al., 2018; Lee et al., 2015; Son et al., 2016) that demonstrated the oxide layer formed on the heater could improve CHF. The oxidized surface superheat of ONB and CHF showing in Fig. 6 is smaller than that of fresh tube while this is reversed in the cases as shown in Figs. 3, 4 and 5. However, the various flow boiling conditions may attribute to the mechanistic rationales behind the superheat difference of ONB and CHF between the fresh and oxidized tube.

Generally, in the experimental results presented in Figs. 3 to 6, the flow boiling curves of oxidized specimens shift rightward in comparison with those of their non-oxidized counterparts. This implies that the presence of oxide layer deteriorates the boiling heat transfer and results in the higher wall superheat. Although the presence of oxide layer can result in the CHF enhancement, it also brings a deterioration of boiling heat transfer coefficient by adding a thermal resistance to the surface. Similar experimental observations were also reported in the flow boiling CHF experiments of carbon steel (Wang et al.,2020). It was reported in several CHF experimental studies that the oxidized samples can enhance flow boiling CHF (He et al., 2021) and the CHF occurrence superheat of oxidized samples is usually higher than that of their non-oxidized counterparts. One explanation is that the presence of an oxide layer devastates the heat dissipation ability of the triple-phase surface from the heater solid to the liquid-vapor mixture because of the degraded thermal conductivity of oxides. This is also in confirmation with our experimental results (Figs. 3, 4, and 5). However, the results presented in Fig. 6 contradict with the previous experimental findings. This speaks to that the cladding surfaces that are oxidized by the surface

temperature overshooting of CHF occurrence can shift the flow boiling curve upward and leftward, and the related mechanisms are more complicated. The results presented in Fig. 6 imply that there are at least two different competing mechanisms resulting from the oxide layer, surface wettability enhancing nucleate boiling heat transfer coefficient while an oxide layer can deteriorate it, resulting in temperature decrease for the oxidized tube. The flow boiling experiments, as shown in Fig. 7, have the inlet subcooling of 0 °C and the dryout type CHF occurs on the SS 316 tubes. The results indicate that the dryout gain by increasing mass flux is limited in the fresh SS 316 tubes, while the oxide layer can magnify the dryout gain resulting from higher mass fluxes. For the DNB of flow boiling in Fig. 8, the DNB of oxidized tubes is augmented at least 15% compared with that of fresh tubes. Different from the dryout enhancement, the enhancement ratio of DNB by oxide layer is weak under both low and high mass fluxes but is more pronounced at the intermediate mass fluxes. As can be seen in Fig. 9, the higher inlet subcooling, the higher the enhancement effect on flow boiling CHF of oxidized tubes.

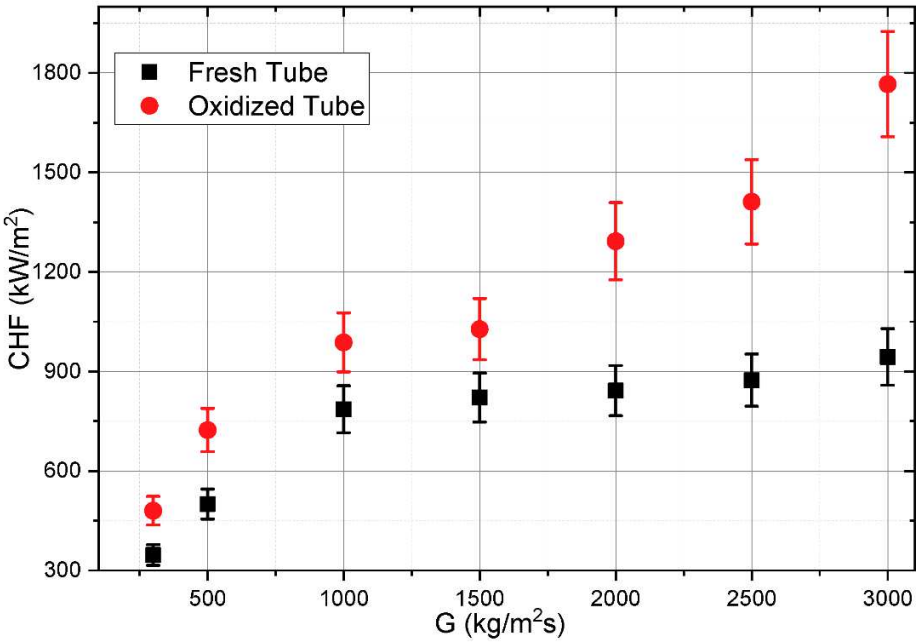

Fig. 7. Flow Boiling CHF of Fresh and Oxidized SS 316 Tubes with ΔT_{sub} = 0 °C under Different Mass Fluxes.

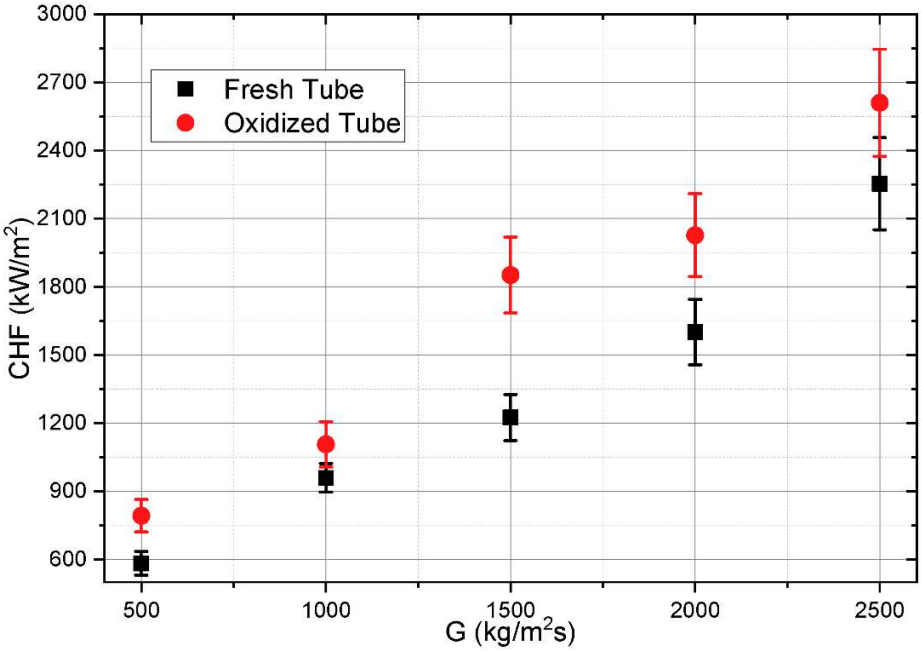

Fig. 8. Flow Boiling CHF of Fresh and Oxidized SS 316 Tubes with ΔT_{sub} = 10 °C under Different Mass Fluxes.

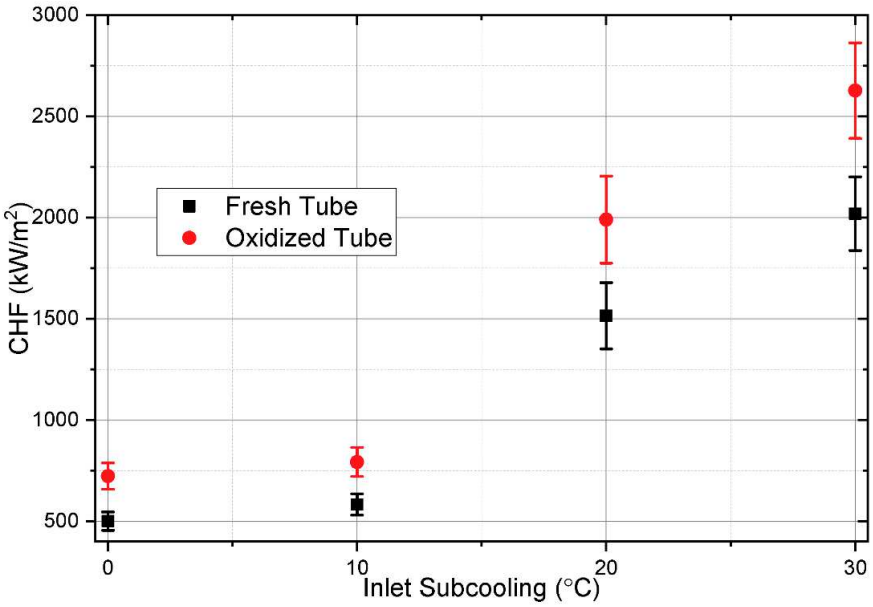

Fig. 9. Flow Boiling CHF of Fresh and Oxidized SS 316 Tubes with G = 500 kg/m^{2}s under Different Inlet Subcooling.

However, as shown in Fig. 10, the flow boiling CHF of oxidized Inconel 600 is smaller than that of fresh Inconel 600 sample. Also, the flow boiling curves of oxidized Inconel 600 shift leftward in comparison with the flow boiling curve of the non-oxidized Inconel 600. The experimental results of Inconel 600 contradict those of SS 316. This speaks to the possibility that the effects of oxide layers on flow boiling depends on the tested sample substrate materials and the

microstructure of the formed oxide layer. It should be noted that the flow boiling CHF of Inconel 600 is higher than that of SS 316 due to the dominant effect of material properties. Because of the low mass flux and high inlet temperature, the effects of material thermal-physical properties on flow boiling CHF could be dominant. Similar experimental investigations on flow boiling CHF difference between various materials can be found in Ref. (He et al., 2021). It is noted that a fresh tube is an as-received sample that is sandblasted by a sandpaper. The first oxidized tube is a fresh sample that experiences the surface temperature overshooting of CHF occurrence only once, and the second oxidized tube is the first oxidized sample with CHF-reoccurrence on the post-CHF surface.

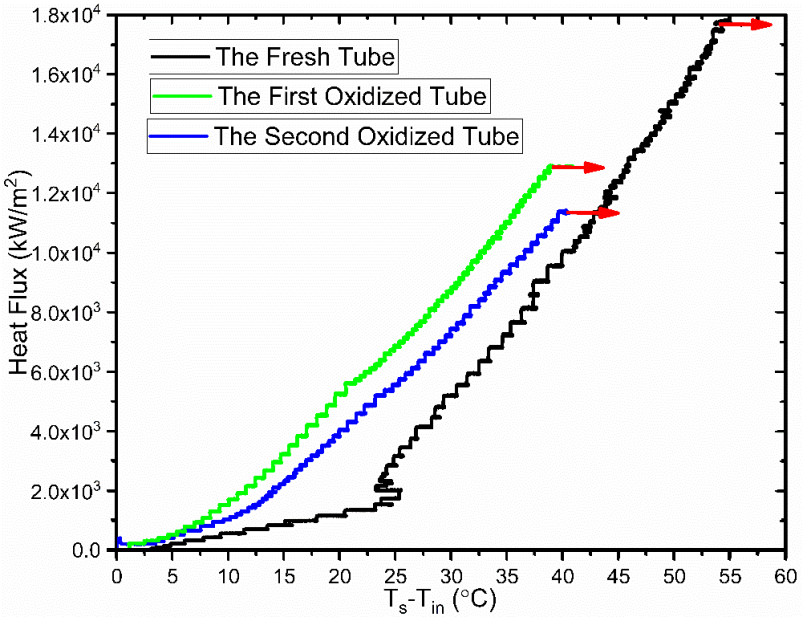

Fig. 10. Flow Boiling Curve of Fresh Inconel 600 and its Oxidized Tubes with G = 500 kg/m^{2}s and ΔT_{sub} = 0 °C.

3.2 Analyses of Surface Morphologies

Fig. 11 shows the SEM micrographs of both fresh and oxidized tube surfaces. It is expected that the non-heated fresh SS 316 tube shows no obvious characteristics, as shown in Fig. 11(a). Fig. 11(b) presents the morphological evidence of surface cracks but no clear formation of oxide layer for the flow boiling case of G = 500 kg/m^{2}s and ΔT_{sub}=0 °C. However, as progressively increasing the inlet subcooling showing in Figs. 11(c) and (d), the layers of surface oxides are formed on the inner surfaces of SS 316 specimens. Comparing the morphological structures of oxide crystals of various heated samples in Figs. 11(c) and (d) illustrates that the oxide crystal structure becomes finer by increasing inlet subcooling. This implies that inlet subcooling can affect the formation of oxide crystals and the morphological structures of oxide layer. There are some areas that are not covered by oxide crystals presenting on the inner surfaces of oxidized samples, which is due to the fact that the intense mechanical vibrations chopped off some oxide layers from the surfaces during sample preparation.

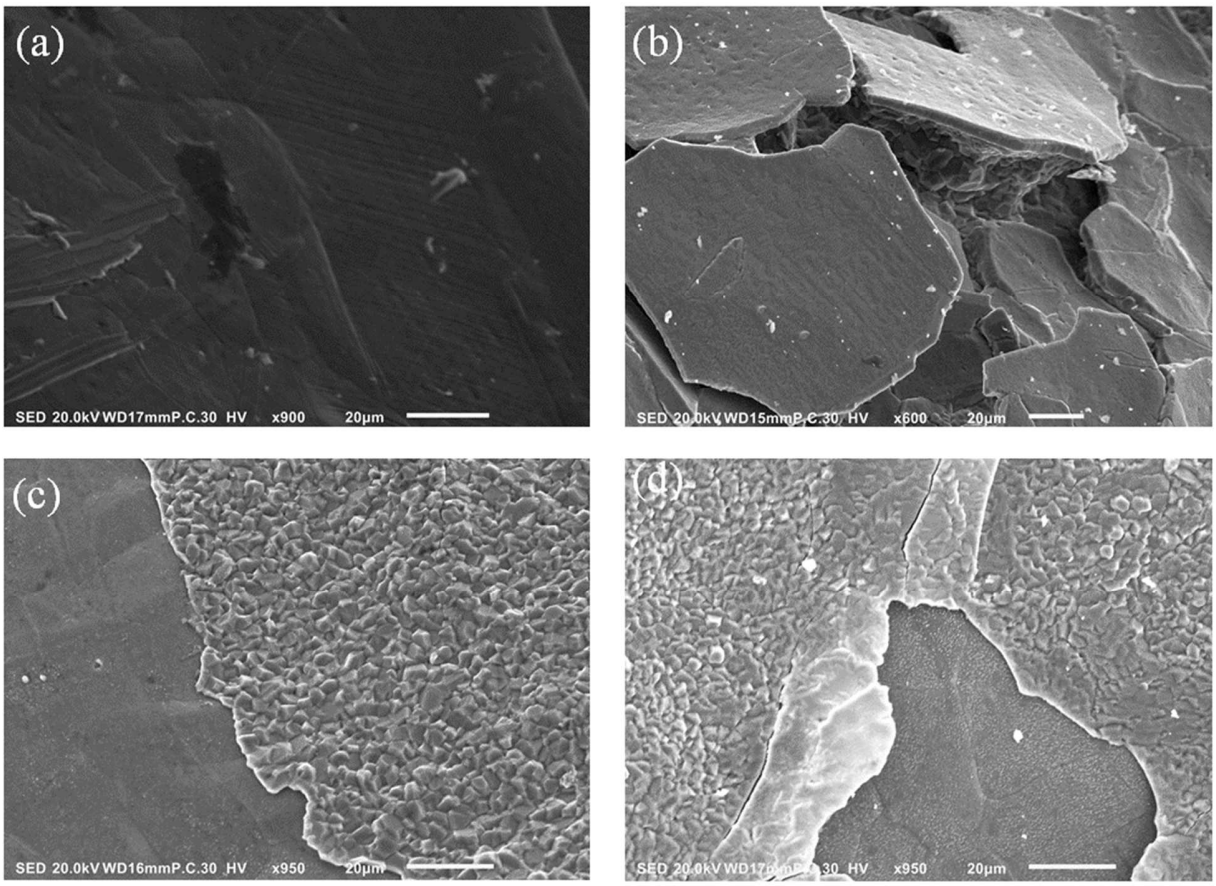

Fig. 11. SS 316 Specimen: (a) As-Received, (b) G = 500 kg/m^{2}s and ΔT_{sub} = 0 °C, (c) G = 500 kg/m^{2}s and ΔT_{sub} = 10 °C, and (d) G = 500 kg/m^{2}s and ΔT_{sub} = 20 °C.

On the other hand, Fig. 12 demonstrates differences in surface morphologies between oxidized specimens under different mass flux but the same subcooling. Fig. 12 shows that the morphological structure sizes of surface oxide crystals become finer, and the distribution of oxide clusters is more densely compacted as mass flux increases. This indicates that mass flux can contribute to the oxidized surface morphological patterns formation.

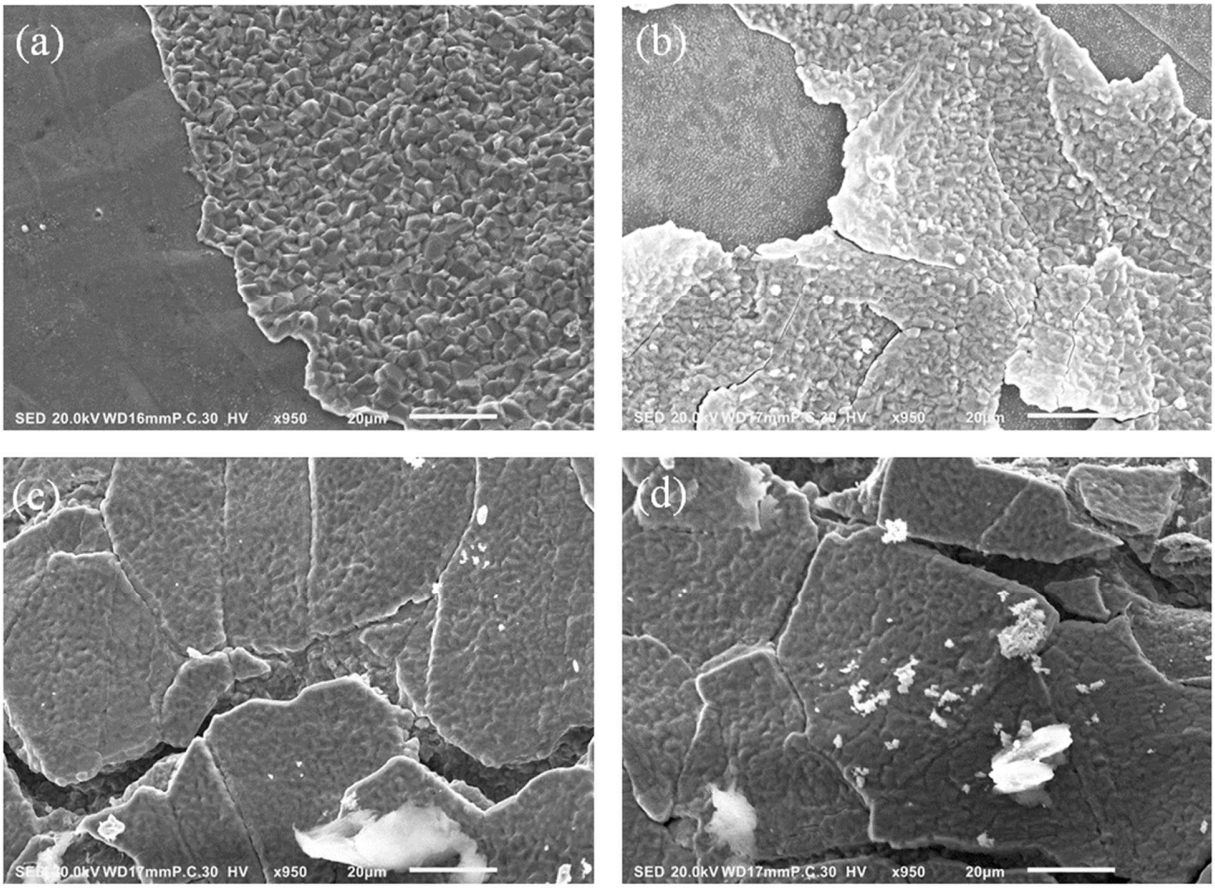

Fig. 12. SS 316 Specimen: (a) G = 500 kg/m^{2}s and ΔT_{sub} = 10 °C, (b) G = 1000 kg/m^{2}s and ΔT_{sub} = 10 °C, (c) G = 1500 kg/m^{2}s and ΔT_{sub} = 10 °C, and (d) G = 2000 kg/m^{2}s and ΔT_{sub} = 10 °C.

For the steady-state flow boiling, there are two distinct segments in a tested tube, non-oxidized and oxidized, as shown in Fig. 13, and flow boiling CHF usually occurs at proximity close to the outlet because of vapor quality. Surface morphologies of four different axial locations (respectively marked from *a* to *d* in Fig. 13) are also investigated on the same oxidized test specimen of the SS 316 tube. Fig.14 evidently illustrates that surface morphological patterns along the axial direction of the tested specimen could be divided into four distinct genres based on the structures of oxide crystals. At point (a), the oxides are sparsely distributed on the surface, as can be seen in Fig. 14(a), where the structural size of oxides is too small to be compacted together to cover the surface implying that oxides are still under the growth stage. As the vapor quality increases axially along the tested tube, surface oxides gradually build up and densely compact together to cover the surfaces, as shown in Fig. 14(b). The compacted surface oxides cluster together to form bigger oxide crystalline structures, which can be seen in Fig. 14(c). The further progressively-increased vapor quality makes these densely-clustered crystalline structures to form a thin layer of oxide on the surface, as observed in Fig. 14(d).

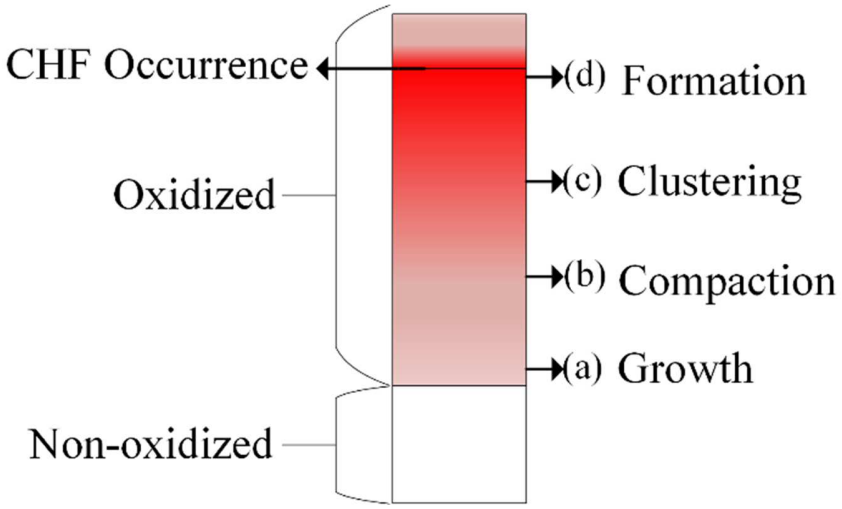

Fig. 13. Illustration of the Oxidized SS 316 Tube under the Inlet Subcooling of 30 °C.

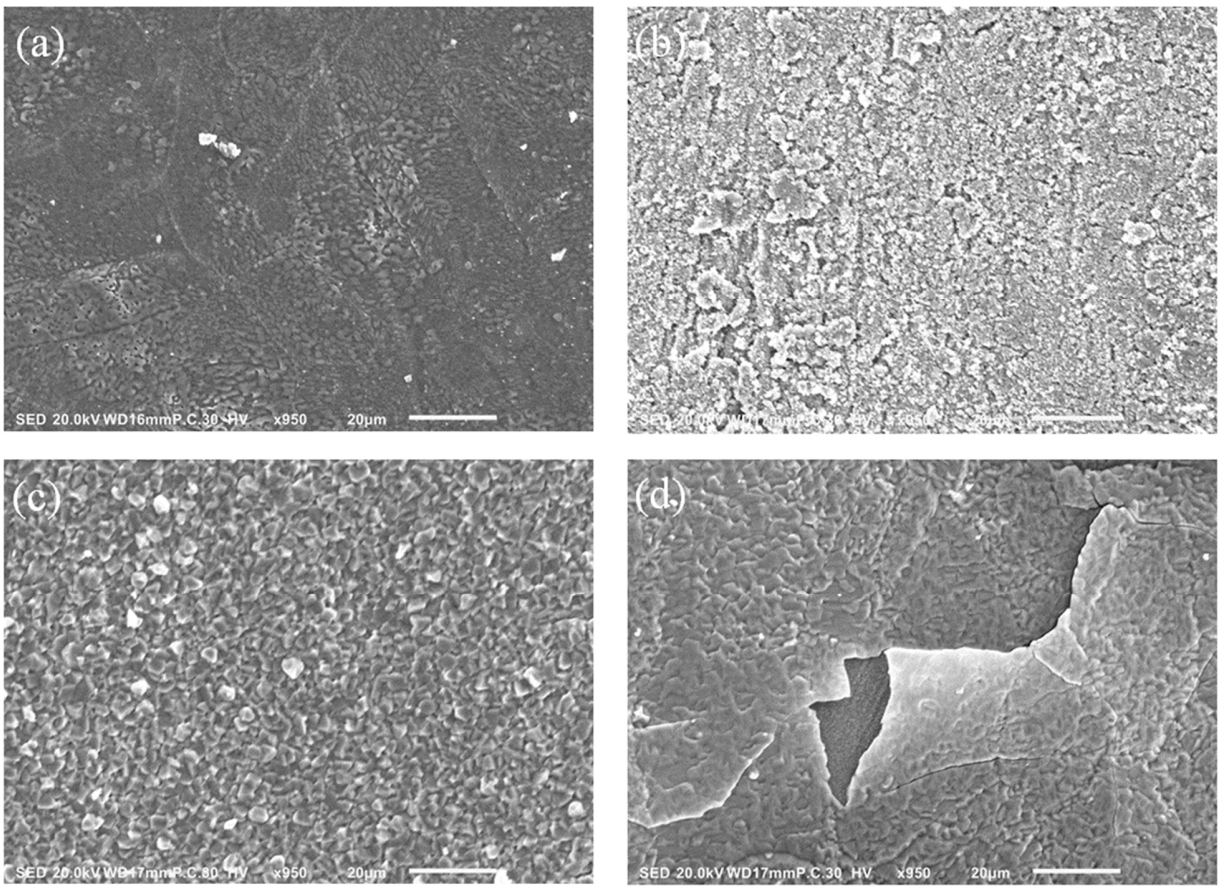

Fig. 14. Specimens at four Different Axial Locations in a SS 316 Tube Oxidized by CHF of G = 500 kg/m^{2}s and ΔT_{sub} = 30 °C: (a) Growth, (b) Compaction, (c) Clustering, and (d) Formation.

Different from flow boiling CHF on SS 316 tubes, temperature overshooting on Inconel 600 tubes does not form oxide crystals Moreover, the only difference incurred by the surface temperature overshooting of CHF occurrence is a different presence of surficial textures, as shown in Fig. 15.

In comparisons with the post-CHF surfaces of SS 316, there are neither oxide-crystal clustered nor oxide-layer fractured micro-structured reflected in the post-CHF surface of Inconel 600 (See Fig.15 (b)). On the other hand, the temperature overshooting of CHF occurrence can unavoidably oxidize Inconel 600 samples for flow boiling experiments. However, given that Inconel 600 is more corrosion-resistant than SS 316, and the Cr_2O_3 layer is less susceptible to the fractured damage during film boiling than the Fe_2O_3/Fe_3O_4 layer of SS 316. The cross-section SEM scans are performed to compare the oxide layer presences on the post CHF surfaces of SS 316 and Inconel 600, respectively. Fig. 16 clearly supports the rationale that Inconel 600 has better corrosion resistance to surface temperature overshooting. The intrinsic material thermal-mechanical properties of two different oxide layers might indicate that the Fe_2O_3/Fe_3O_4 layer is more fragile to fracture than the Cr_2O_3 layer.

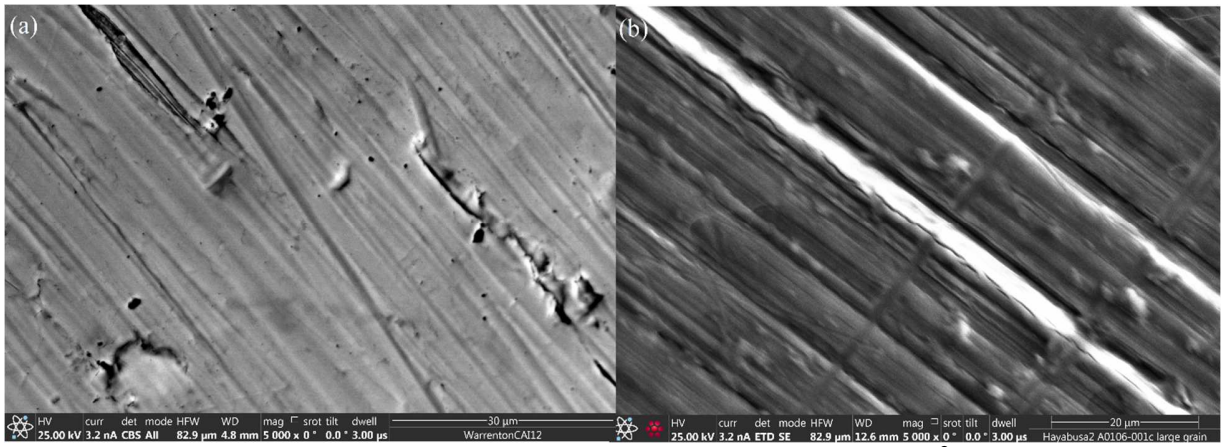

Fig. 15. Inconel 600 Specimens: (a) As-Received and (b) G = 500 kg/m^{2}s and ΔT_{sub}=0 °C.

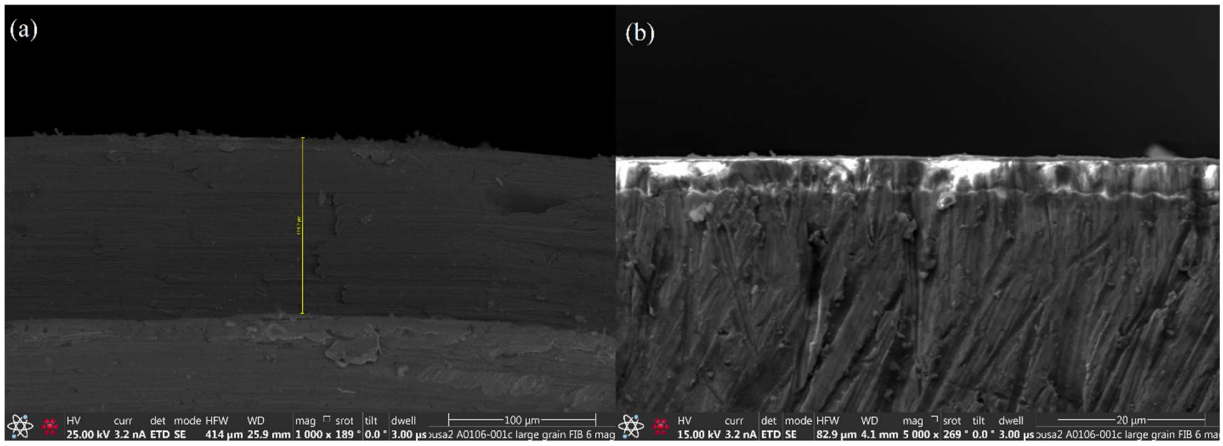

Fig. 16. Radial Cross-Sectional SEM Scans on the Oxide Layers of (a) SS 316 and of (b) Inconel 600 at G = 500 kg/m^{2}s and ΔT_{sub}=0 °C.

3.3 Surface Wettability Analyses of Post-CHF Surfaces

The SEM scan analyses of post-CHF surfaces demonstrate that the introduction of oxide layers, resulted from surface temperature shooting, could explain the CHF enhancement/deterioration on the post-CHF surfaces. The presence of oxide layers can have significant impacts on surface

wettability, nucleation site densities, and micro-structured morphologies. To obtain the effects of surface wettability change on the post-CHF surfaces, the contact angles of tested samples are procured before and after the boiling experiments. Standard criteria and procedures are followed to measure contact angles on tested samples. For example ASTM D7334 was followed in the pool boiling experiments using ATF materials (Ali et al., 2018). However, the measurement methodology of contact angles on curved surfaces is not technically available. Guilizzoni proposed a semi-empirical correlation to correct the effect of convex curvature on contact angles (Guilizzoni, 2011). For a convex surface showing in Fig. 17, the curvature effects are minimized by the minimal allowable sized de-ionized water droplet using a goniometer (Lee et al., 2019). In this study, the measurement method used by Lee et al. (2019) is adopted due to its simplicity. As observed in Fig. 17, at a point of triple phases, two mutually normal vectors are established as a reference frame, and the static contact angle is the one between the vector that points towards the bottom and the tangent vector that passes along the concave direction of a 5 μL water droplet. Based on Kandlikar's CHF model (Kandlikar, 2001), the receding contact angle is the study of interest that explains the effect of surface wettability on CHF. The contact angle Goniometer (rame-hart) can measure both advance and receding contact angles by changing the specimen tilting angles and using the automated tilting base. However, such a measurement method is not applicable to the curved surfaces with upwardly-faced curvature due to the displacement of specimen on a tilting base. The static contact angle is used as an indicator of surface wettability of oxidized samples in this study, and it is measured on the as-received and post-CHF surfaces. The corresponding measurement procedures are in accordance with the standard of American Society of Testing Materials (ASTM, 2013). The ambient temperature of contact angle measurement is approximately close to the inlet temperature of water coolant, and the tested specimens are put in a transparent chamber where the ambient temperature is controlled by the contact angle Goniometer. The surrounding gas medium of the transparent chamber is the dry air. To minimize the volume shrinkage of water droplet, five measurements are performed on each sample within 5 secs respectively.

Figs. 18(a) and (b) present the static contact angle on different post-CHF surfaces that are oxidized under various flow boiling conditions. The post-CHF oxidized surfaces become progressively hydrophobic and have less surface wettability when increasing the inlet subcooling or mass flux.

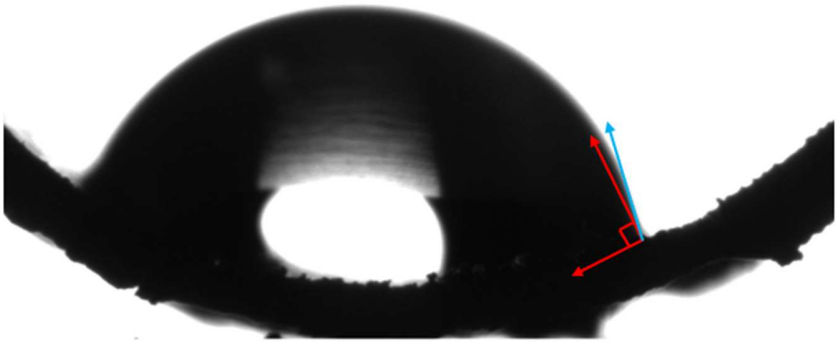

Fig. 17. Static Contact Angle on a Curved Surface of Post-CHF SS 316.

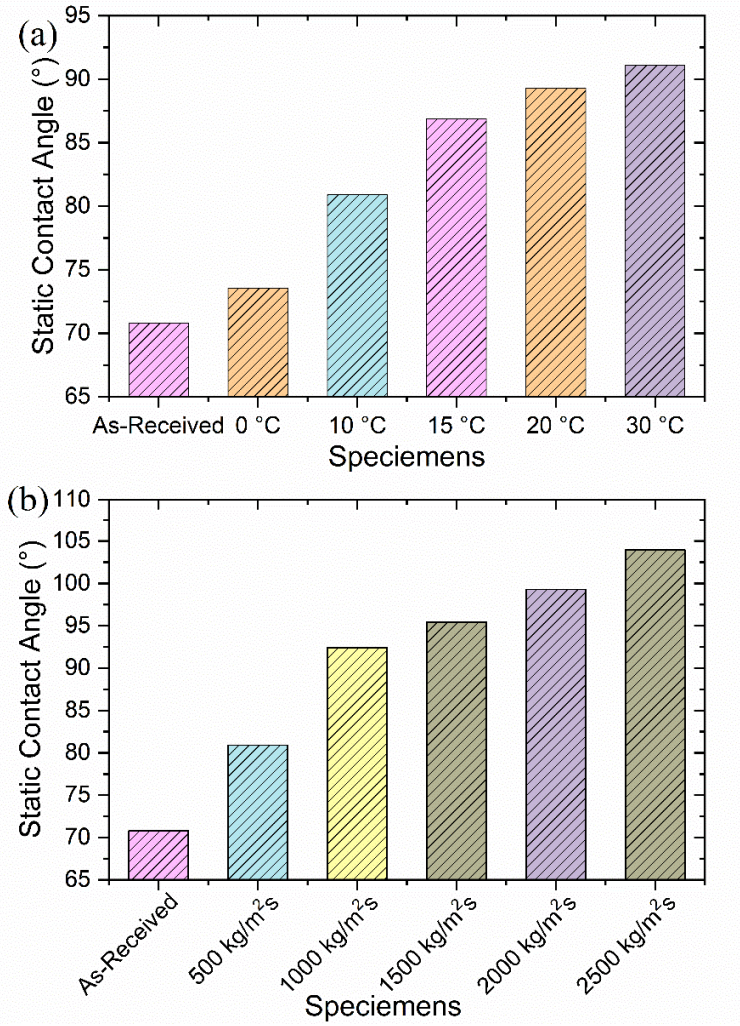

Fig. 18. Static Contact Angles of Curved SS 316 Specimens under Various Flow Boiling Conditions: (a) G = 500 kg/m^{2}s and Different Inlet Subcooling and (b) ΔT_{sub} = 10 °C and Different Mass Fluxes.

Without incorporating the effect of thermal-physical properties, the hydrophobic boiling surfaces with less surface wettability can deteriorate CHF. Therefore, this physical rationale could not support CHF enhancement on hydrophobic oxidized surfaces of SS 316. The other plausible cause resulting in CHF enhancement may originate from the micro-structured morphologies formation of oxide layer on surfaces and the change in thermal-physical properties.

On the opposite to flow boiling cases using SS 316 material, CHF deteriorates on the post-CHF surfaces of Inconel 600 that have better surface wettability, as shown in Fig. 19. This surface wettability enhancement result on the post-CHF surface of Inconel 600 is in agreement with experimental investigations to the effects of oxidation on contact angle (Hong et al., 1994), that is, surface oxidization does decrease the contact angles of liquid droplet and enhance surface wettability. However, this contradicts with the increasing of post-CHF SS 316 surface contact angles. The micro-structured morphologies of oxide crystals indicate the possible rationale behind this contradictory as there are no noticeable oxide micro-structures on the Inconel 600 post-CHF

surfaces, and moreover metal oxides are generally hydrophilic owing to metal cations, oxygen anions, and hydroxyl groups on the surface. One of the theoretical explanations behind the surface wettability devastation by the micro-structured surface is that air pockets that are entrapped by the micro-structured gaps repel away the water droplets and reduce the capillary penetration ability of water molecules, as can be seen in Fig. 20. Although the oxide micro-structured morphologies of SS 316 post-CHF surfaces are not in a specific pattern, it is plausible to explain that the contact angles of SS 316 post-CHF surfaces are higher than that of the non-oxidized SS 316 surfaces.

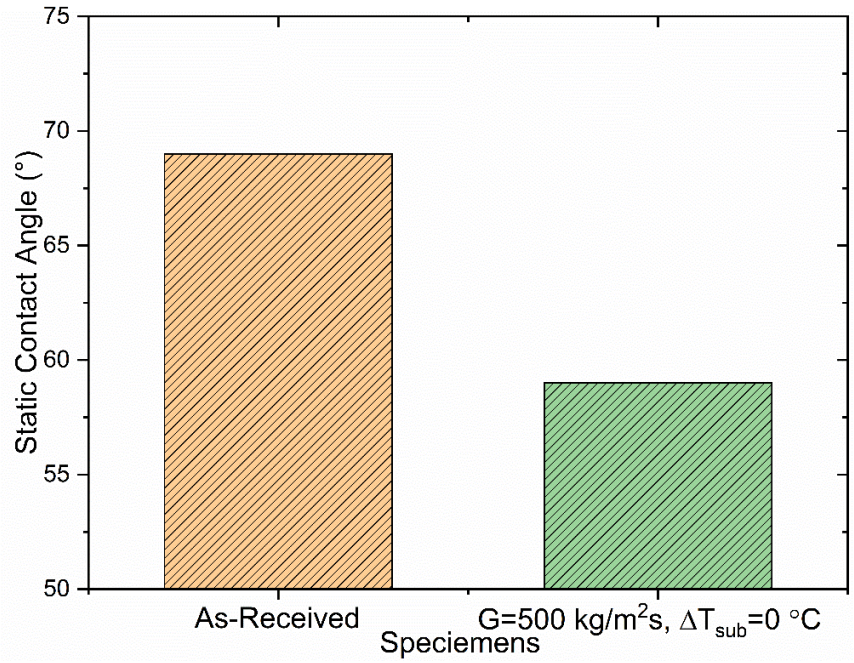

Fig. 19. Static Contact Angles of Inconel 600 Specimen.

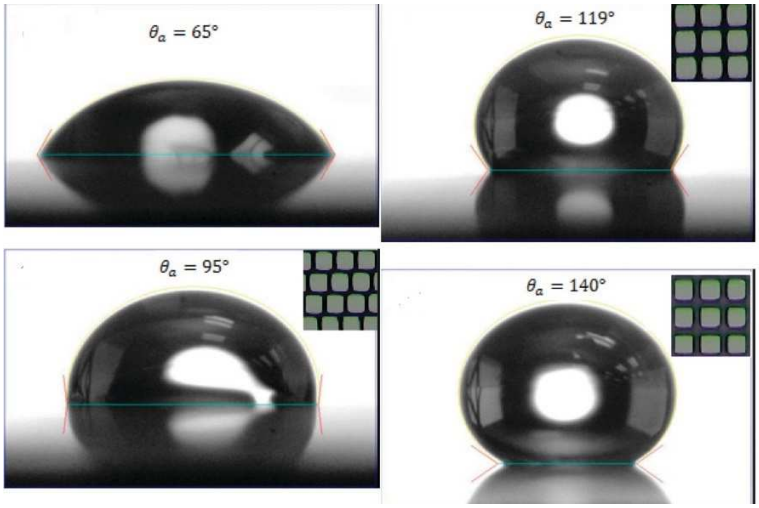

Fig. 20. Contact Angles on a Flat Smooth Surfaces and Three Different Micro-Structured Surfaces (Kashaninejad et al. (2012)).

3.4 Mechanistic Analyses on CHF Enhancement

After the post-CHF oxidization, the static contact angle of SS316 tested increases, while the Inconel 600 has a smaller static contact angle. This contradicts with most experimental investigations to effects of surface oxidization on CHF (Lee et al., 2015; Son et al., 2016; Wang et al.,2020). Different from those studies, the post-CHF surfaces of SS 316 present oxide micro-structured surface morphologies that are produced by the flow boiling instead of pool boiling. This phenomenologically explains why the wettability change of our Inconel 600 post-CHF surface agrees with other experimental results while SS 316 flow boiling oxidized samples show opposite results in this current study. As pointed by Lee et al. (2019), the wettability change resulting from surface oxidization has limited influences on flow boiling CHF unless the tested materials are extremely either hydrophobic or hydrophilic. These experimental investigations imply that the surface wettability variations resulting from oxide layers could contribute to the enhancement/deterioration of pool boiling CHF but have limited impacts on flow boiling CHF. This implies that the surface wettability change resulting from oxide layers could not sufficiently explain the flow boiling CHF enhancement of SS 316.

In this study, two perspectives are considered to explain the CHF amelioration/deterioration: thermal-physical properties and micro-structured surface. In several pool boiling experimental studies, CHF difference gaps between claddings are mechanistically dominated by thermal effusivity that physically quantifies a material's ability to change thermal energy between solids and the surrounding environment. As shown in Table 1, the thermal effusivities of two iron oxides are higher than that of the SS 316. This might partially explain that flow boiling CHF is enhanced on the post-CHF surfaces of SS 316. However, since the oxide layer on SS 316 is much thinner than the wall thickness, the potential impacts of iron oxides thermal effusivity on SS 316 flow boiling CHF enhancement are limited. The most likely enhancement mechanism behind the SS 316 flow boiling CHF in this study is due to oxide micro-structured surface morphologies. As suggested by Kim et al. (2014), the interfacial wicking velocity is pronouncedly improved by micro-pillars to better spread liquid over hot patches and enhance pool boiling CHF. Similarly, the oxide micro-structured surface morphologies on SS 316 post-CHF samples are to improve the capillary wicking ability of prompting liquid supply to hot patches and prevent them from the irreversible formation of dry patches.

Table.1 Thermal-Physical Properties of Inconel 600, SS 316 and Their Oxides (Evaluated at 100°C)

Material	Mass Density (kg/m^3)	Thermal Conductivity (W/(m·K))	Heat Capacity (J/(kg·K))	Thermal Effusivity $(\rho k c_p)^{0.5}$	Thermal Diffusivity $k/(\rho c_p)$ mm^2/s
Inconel 600	8470	15.89	464.97	7910.72	4.03
SS 316	7921	15.11	508.86	7804.07	3.75
Chromia Cr_2O_3	5210	8.23	736.88	5621.04	2.14
Hematite Fe_2O_3	5302	5.92	10762.12	18379.31	0.11
Magnetite Fe_3O_4	5150	3.72	44626.27	37426.22	0.02

Although the layer thickness of Cr_2O_3 is roughly several microns, the decreasing of thermal-effusivity owing to the oxide could not be sufficiently explained CHF deterioration of Inconel 600. On the other hand, the non-micro-structured oxide layer can have influential impacts on the site density of active nucleation because the presence of oxide layer significantly deteriorates the

thermal diffusivity of cladding surface on which bubbles are generated and boiling occurs on. Because thermal diffusivity measures the ability of a material to conduct thermal energy relative to its ability to store thermal energy. During the nucleation and growth of bubbles, the water bulks absorb thermal energy conducted by the boiling surface and vaporize in a vapor mini region. The decreasing of boiling surface thermal diffusivity results in a significant reduction of active nucleation sites even though the oxide layer is roughly several microns thick. As pointed out by Kandlikar (2006) and Wang et al. (2018), the decreasing of active nucleate site density leads to the possible deteritation of CHF. With the micro-structure enhanced capillary wicking effect, the oxide layer could explain that pool boiling CHF is detetiorated in some reported experiemental studies of oxdizied samples (Son et al., 2016) and of ceremics-coated samples (Kam et al., 2015). As a result of these dicussions, the flow boiling CHF deterioation of Inconel 600 post-CHF could be rationalized by the non- microstructured oxide layer. The surface roughness of the tested samples has dominant roles in pool boiling CHF (Son et al., 2016; Yeom et al., 2020), while Hata et al. (2004, 2006) found that no significant influence of surface roughness on flow boiling CHF was observed on the tested materials of SS 304. This might imply that the surface roughness change owing to the Cr_2O_3 layer could not explain the flow boiling differences between the non-oxidized and post-CHF surfaces, neither surface wettability (Seo and Bang, 2015), nor surface wickability (Kim et al., 2014).

The corresponding physics understanding is not technically ready. This needs the future development and progress of material-conjugated boiling heat transfer. As pointed in the review study of ATF cladding boiling heat transfer experiments (He et al., 2021), speaking from the interfacial physics viewpoints, the phase change of nucleate boiling may involve with solid-liquid/solid-vapor heat conduction/radiation and heat dissipation and absorption capability of the composite substrates of non-oxides and oxides could result in the deciding impacts on the irreversible formation of dry patches. Therefore, in this study, it is difficult to rationalize whether either the hydrodynamics-related factors, including surface capillary forces, surface wettability, and etc., or the thermal-physical factors, including thermal diffusivity, thermal effusivity, thermal activity, and etc., contribute to the CHF amelioration/ deterioration resulting from the presence of oxide layer.

3.5 Implications of Experimental Results

However, in Fig.10, the flow boiling CHFs of oxidized Inconel tests are smaller than that of the fresh Inconel sample, while the flow boiling CHF of the twice-oxidized sample is greater than that of the once-oxidized sample. The similar experimental results were also reported on the flow boiling CHF experiments of Inconel 625 (Suk et al., 2020), in which the effect of oxide layer was briefly studied. It should be noted that although the presence of SS-316 oxide layer has a positive contribution to flow boiling CHF, it deteriorates the flow boiling heat transfer coefficients and further results in the PCT. However, this phenomenon is reversed in the flow boiling of Inconel 600. The presence of the Inconel 600 oxide layer can lead to a lower PCT. The implications of experimental results are that (1) the effects of oxide layer on flow boiling CHF are determined by two dominant factors, claddings' thermal-physical/mechanical properties and the micro-structured surface morphologies of oxides, and (2) the role of surface wettability is insignificant to the contribution of flow boiling CHF enhancement. These experimental results also speak to that the safety margins, thermal-hydraulic performances, mechanical integrities of fuel claddings may demonstrate distinct behaviors due to reactor operation histories and their footprints on claddings.

Although the mechanical integrity of ATF candidates could improve the safety margins for LWRs, the post-accident core materials can very likely present different material compositions of cladding surface and show beyond-estimation safety margins, especially cladding materials. For example, the cladding surface of FeCrAl is covered by a thin layer of Cr_2O_3 under the normal operations and by a thick layer of Al_2O_3 during the accidental scenarios (Gupta et al., 2018; Rebak et al., 2016). Due to the formation of oxide layers on the cladding surface, the mode of boiling heat transfer is very likely conjugated with material compositions of claddings. Thus, the experimental CHF data that are procured on as-received non-heated materials could not support the safety evaluation of core-loaded claddings. Compared with the thermal power safety margin, the thermal concerns of PCT should be more addressed for the corrosion limit of ATF claddings. This experimental study along with the recent progresses of ATF cladding boiling experiments (He et al., 2021) gives us new insights on the material-conjugated boiling heat transfer by looking at how the oxide layer affects boiling heat transfer of cladding materials. Comparative experiments on non-oxidized materials, oxide-coating materials, and corresponding oxide-ceramics materials, such as Cr/Cr_2O_3-coating/ Cr_2O_3 ceramics, Al/Al_2O_3-coating/Al_2O_3 ceramics, Si/SiO_2-caoting/Silica, Zr/Zr-coating/ZrO_2 ceramics, will need to be carried out. This intrinsic strategy of flow boiling CHF enhancement is more feasible for the safety analyses of LWRs using ATF without significant modifications of operation protocols in comparisons with other enhancement techniques such as wire heaters (Guo et al., 2021), and nanofluids (Wang et al., 2021).

4 CONCLUSIONS

This study presents how the temperature overshooting led by CHF occurrence on as-received tubes can have influential impacts on CHF re-occurrence on post-CHF surfaces. Experimental results of SS 316 tubes reveal that flow boiling CHF on post-CHF surfaces is significantly enhanced. Also, as increasing the mass flux and/or inlet subcooling, the degree of CHF enhancement can be further advanced. The SEM micrographs of post-CHF SS 316 surfaces could support the idea that formation of oxide layer contributes to CHF enhancement on post-CHF hydrophobic materials with less surface wettability. These post-CHF oxidized surfaces will become more hydrophobic if either mass flux or inlet subcooling is increased. However, the flow boiling experiments of Inconel 600 shows opposite behaviors to that of SS 316: CHF on post-CHF surface has deteriorated, the post-CHF surface is more hydrophilic than the as-received sample, and a non-microstructure layer of oxide is formed on boiling surface. CHF difference between as-received and post-CHF surfaces could be rationalized by the changes of material thermal-physical properties and of surface morphologies. This implies that the evolutionary changes of cladding surfaces can affect the thermal-hydraulic performances during the reactor lifetime. Therefore, it is imperative to keep track of cladding material surface changes during the entire period of core-loading, especially for FeCrAl claddings that can present various surface morphologies and material compositions.

ACKNOWLEDGEMENTS

This material is based upon work supported by the U.S. Department of Energy Office of Nuclear Energy's Nuclear Energy University Program under award number DE-NE0008687 and Integrated Research Program under award number DE-NE-0008531.

REFERENCES

Ali, A.F., Gorton, J.P., Brown, N.R., Terrani, K.A., Jensen, C.B., Lee, Y., Blandford, E.D., 2018. Surface wettability and pool boiling Critical Heat Flux of Accident Tolerant Fuel cladding-FeCrAl alloys. Nucl. Eng. Des. 338, 218–231. https://doi.org/10.1016/j.nucengdes.2018.08.024

ASTM, 2013. Standard Practice for Surface Wettability of Coatings, Substrates and Pigments by Advancing Contact Angle Measurement.

Carrica, P.M., Leonardi, S.A., Clausse, A., 1995. Experimental study of the two-phase flow dynamics in nucleate and film pool boiling. Int. J. Multiph. Flow 21, 405–418. https://doi.org/10.1016/0301-9322(94)00076-V

Chen, M., Sun, X., Christensen, R.N., Skavdahl, I., Utgikar, V., Sabharwall, P., 2018. Dynamic behavior of a high-temperature printed circuit heat exchanger: Numerical modeling and experimental investigation. Appl. Therm. Eng. 135, 246–256. https://doi.org/10.1016/j.applthermaleng.2018.02.051

Cheng, T., Keiser, J.R., Brady, M.P., Terrani, K.A., Pint, B.A., 2012. Oxidation of fuel cladding candidate materials in steam environments at high temperature and pressure. J. Nucl. Mater. 427, 396–400. https://doi.org/10.1016/j.jnucmat.2012.05.007

Guilizzoni, M., 2011. Drop shape visualization and contact angle measurement on curved surfaces. J. Colloid Interface Sci. 364, 230–236. https://doi.org/10.1016/j.jcis.2011.08.019

Gupta, V.K., Larsen, M., Rebak, R.B., 2018. Utilizing FeCrAl Oxidation Resistance Properties in Water, Air and Steam for Accident Tolerant Fuel Cladding. ECS Trans. 85, 3–12. https://doi.org/10.1149/08502.0003ecst

Guo, K., Wang, C., Zhang, D., Tian, W., Su, G., Qiu, S., 2021. Investigations of near-wall bubble behavior in wire heaters pool boiling. Thermal Science. 5 Part B, 3957-3967. https://doi.org/10.2298/TSCI200408333G

Hata, K., Shiotsu, M., Noda, N., 2004. Subcooled Flow Boiling Critical Heat Flux in Short Vertical Tube: Influence of Inner Surface Roughness. 2004 ASME International Mechanical Engineering Congress and Exposition. IMECE2004-61453, 653-662. https://doi.org/10.1115/IMECE2004-61453

Hata, K., Shiotsu, M., Noda, N., 2006. Influence of Heating Rate on Subcooled Flow Boiling Critical Heat Flux in a Short Vertical Tube. JSME Int. J., Ser. B. 49, 309-317. https://doi.org/10.1299/jsmeb.49.309

He, M., Lee, Y., 2018. Application of machine learning for prediction of critical heat flux: Support vector machine for data-driven CHF look-up table construction based on sparingly distributed training data points. Nucl. Eng. Des. 338, 189–198. https://doi.org/10.1016/j.nucengdes.2018.08.005

He, M., Wang, J., Chen, M., 2021. Recent progresses on thermal–hydraulics evaluations of accident tolerant fuel cladding materials. Ann. Nucl. Energy. 161, 108391. https://doi.org/10.1016/j.anucene.2021.108391

He, Y., Shirvan. K., Wu. Y., Su. G., 2021. Preliminary prediction for survival time of fuel rod under critical heat flux. Ann. Nucl. Energy. 151, 107896. https://doi.org/10.1016/j.anucene.2020.107896

Hong, K. T., Imadojemu, H., Webb, R. L., 1994. Effects of oxidation and surface roughness on contact angle. Exp. Therm. Fluid Sci. 8, 279-285. https://doi.org/10.1016/0894-1777(94)90058-2

Kam, D. H., Lee, J. H., Lee, T., Jeong, Y. H., 2015. Critical heat flux for SiC- and Cr-coated plates under atmospheric condition. Ann. Nucl. Energy. 76, 335-342. https://doi.org/10.1016/j.anucene.2014.09.046

Kam, D.H., Choi, Y.J., Jeong, Y.H., 2018. Critical heat flux on downward-facing carbon steel flat plates under atmospheric condition. Exp. Therm. Fluid Sci. 90, 22–27. https://doi.org/10.1016/j.expthermflusci.2017.08.028

Kandlikar, S.G., 2006. Nucleation characteristics and stability considerations during flow boiling in microchannels. Exp. Therm. Fluid Sci. 30, 441–447. https://doi.org/10.1016/j.expthermflusci.2005.10.001

Kandlikar, S.G., 2001. A Theoretical Model to Predict Pool Boiling CHF Incorporating Effects of Contact Angle and Orientation. J. Heat Transfer 123, 1071. https://doi.org/10.1115/1.1409265

Kashaninejad, N., Chan, W. K., Nguyen, N.-T., 2012. Eccentricity Effect of Micropatterned Surface on Contact Angle. Langmuir. 28, 4793-4799. https://doi.org/10.1021/la300416x

Kim, B.S., Lee, H., Shin, S., Choi, G., Cho, H.H., 2014. Interfacial wicking dynamics and its impact on critical heat flux of boiling heat transfer. Appl. Phys. Lett. 105, 191601. https://doi.org/10.1063/1.4901569

Lee, C.Y., Chun, T.H., In, W.K., 2015. Critical heat flux of oxidized zircaloy surface in saturated water pool boiling. J. Nucl. Sci. Technol. 52, 596–606. https://doi.org/10.1080/00223131.2014.956830

Lee, J., Chang, S. H., 2012. An experimental study on CHF in pool boiling system with SA508 test heater under atmospheric pressure. Nucl. Eng. Des. 250, 720-724. https://doi.org/10.1016/j.nucengdes.2012.05.024

Lee, S.K., Liu, M., Brown, N.R., Terrani, K.A., Blandford, E.D., Ban, H., Jensen, C.B., Lee, Y., 2019. Comparison of steady and transient flow boiling critical heat flux for FeCrAl accident tolerant fuel cladding alloy, Zircaloy, and Inconel. Int. J. Heat Mass Transf. 132, 643–654. https://doi.org/10.1016/j.ijheatmasstransfer.2018.11.141

Mei, Y., Shao, Y., Gong, S., Zhu, Y., Gu, H., 2018. Effects of surface orientation and heater material on heat transfer coefficient and critical heat flux of nucleate boiling. Int. J. Heat Mass Transf. 121, 632-640. https://doi.org/10.1016/j.ijheatmasstransfer.2018.01.020

Morshed, A.K.M.M., Paul, T.C., Khan, J., 2013. Effect of Cu–Al_2O_3 nanocomposite coating on flow boiling performance of a microchannel. Appl. Therm. Eng. 51, 1135–1143. https://doi.org/10.1016/j.applthermaleng.2012.09.047

Olson, R.M., Sparrow, E.M., 1963. Measurements of turbulent flow development in tubes and annuli with square or rounded entrances. AIChE J. 9, 766–770. https://doi.org/10.1002/aic.690090612

Rebak, R.B., Terrani, K.A., Fawcett, R.M., 2016. FeCrAl Alloys for Accident Tolerant Fuel Cladding in Light Water Reactors, in: Pressure Vessels and Piping Conference. https://doi.org/10.1115/PVP2016-63162

Seo, S. Bin, Bang, I.C., 2015. Effects of Al_2O_3 nanoparticles deposition on critical heat flux of R-123 in flow boiling heat transfer. Nucl. Eng. Technol. 47, 398–406. https://doi.org/10.1016/j.net.2015.04.003

Son, H.H., Jeong, U., Seo, G.H., Kim, S.J., 2016. Oxidation effect on the pool boiling critical heat flux of the carbon steel substrates. Int. J. Heat Mass Transf. 93, 1008–1019. https://doi.org/10.1016/j.ijheatmasstransfer.2015.10.047

Suk, L., Petrosyan, T., Stevanka, K., Vlcek, D., Gejdos, P., 2020. Experimental Investigation of

Critical Heat Flux on Different Surfaces at Low Pressure and Low Flow. Energies. 13, 5205. https://doi.org/10.3390/en13195205

Trojer, M., Azizian, R., Paras, J., McKrell, T., Atkhen, K., Bucci, M., Buongiorno, J., 2018. A margin missed: The effect of surface oxidation on CHF enhancement in IVR accident scenarios. Nucl. Eng. Des. 335, 140–150. https://doi.org/10.1016/j.nucengdes.2018.05.011

Umretiya, R. V., Vargas, S., Galeano, D., Mohammadi, R., Castano, C. E., Rojas, J. V., 2020. Effect of surface characteristics and environmental aging on wetting of Cr-coated Zircaloy-4 accident tolerant fuel cladding material. J. Nucl. Mater. 535, 152163. https://doi.org/10.1016/j.jnucmat.2020.152163

Wang, K., Erkan, N., Okamoto, K., 2020. A study on the effect of oxidation on critical heat flux in flow boiling with downward-faced carbon steel. Int. J. Heat Mass Transf. 147, 118966. https://doi.org/10.1016/j.ijheatmasstransfer.2019.118966

Wang, K., Gong, S., Bai, B., Ma, W., 2017. On the Relation between Nucleation Site Density and Critical Heat Flux of Pool Boiling. Heat Transfer Eng. 39, 1498-1506. https://doi.org/10.1080/01457632.2017.1369836

Wang, Y., Deng, K., Wu, J., Su, G., Qiu, S., 2018. The characteristics and correlation of nanofluid flow boiling critical heat flux. Int. J. Heat Mass Transfer. 122, 212-221. https://doi.org/10.1016/j.ijheatmasstransfer.2018.01.118

Wang, Y., Wu, J., Yan, X., Su, G., Qiu, S.,2021. An Innovative Method for the Theoretical Investigation on the Critical Heat Flux of Nanofluid Flow Boiling With Nanoparticle Deposition. SSRN. http://dx.doi.org/10.2139/ssrn.3879084

Yeom, H., Gutierrez, E., Jo, H., Zhou, Y., Mondry, K., Sridharan, K., Corradini, M., 2020. Pool boiling critical heat flux studies of accident tolerant fuel cladding materials. Nucl. Eng. Des. 370, 110919. https://doi.org/10.1016/j.nucengdes.2020.110919

Zhang, R., Cong, T., Su, G., Wang, J., Qiu, S., 2020. Investigation on the critical heat flux in typical 5 by 5 rod bundle at conditions prototypical of PWR based on CFD methodology. Appl. Therm. Eng. 179, 115582. https://doi.org/10.1016/j.applthermaleng.2020.115582

Zinkle, S.J., Terrani, K.A., Gehin, J.C., Ott, L.J., Snead, L.L., 2014. Accident tolerant fuels for LWRs: A perspective. J. Nucl. Mater. 448, 374–379. https://doi.org/10.1016/j.jnucmat.2013.12.005